

**AIAA-98-0776**

**Planar Laser Imaging of High-Speed  
Cavity Flow Dynamics**

Ö. H. Ünalmiş, N. T. Clemens, and D. S. Dolling  
Center for Aeromechanics Research  
The University of Texas at Austin  
Austin, Texas 78712-1085

**36th Aerospace Sciences  
Meeting & Exhibit**  
Jan 12-15, 1998 / Reno, NV

# Planar Laser Imaging of High Speed Cavity Flow Dynamics

Ö. H. Ünal mis,\* N. T. Clemens,† and D. S. Dolling‡

Center for Aeromechanics Research  
Department of Aerospace Engineering & Engineering Mechanics  
The University of Texas at Austin  
Austin, Texas 78712-1085

## Abstract

Simultaneous Planar Laser Scattering (PLS) imaging and fluctuating pressure measurements have been made for a rectangular cavity in a Mach 5 turbulent boundary layer. Preliminary results are presented in the form of instantaneous side view images, and power spectra for cavity length-to-depth ratios of 3, 4, 6, 7, and 8. High-frequency response pressure transducers were installed in the rear and front walls of the cavity to monitor the shear layer impingement at the top of the rear wall, and to determine the upstream propagation time of acoustic waves from space-time-correlations. Instantaneous side view PLS images show the impingement shock and expansion waves, whereas the large turbulent structures at the outer edge of the shear layer mask the deflection of the shear layer into the cavity, even for the largest cavity tested. Preliminary analysis of the fluctuating pressure data suggests that the shock frequencies and the duration of the impingement shock are not sensitive to cavity length-to-depth ratio.

## Introduction

Storage of weapons in internal bays of military aircraft offers many potential benefits, including greater maneuverability, higher penetration speed, enlarged flight envelope, elimination of weapon aerodynamic heating, and reduced radar cross section, all of which can enhance aircraft survivability. However, opening weapons bay doors at high speed can result in strong flow instabilities within the bay (or cavity), which induce intense fluctuating pressures in and around the cavity.<sup>1-5</sup> The cavity pressure fluctuations consist of both "broadband" small amplitude pressure fluctuations typical of turbulent shear layers, as well as discrete

resonances whose frequency, amplitude, and harmonic properties depend upon the cavity geometry and external flow conditions. Rizzetta<sup>6</sup> noted that although the mean pressure at approximately the midpoint on the rear wall in an open cavity flow at  $M=1.5$  is only about 30% higher than the freestream static pressure,  $P_\infty$ , peak fluctuating levels can be as much as 2.8 times  $P_\infty$ . Recent work at Mach 5 at The University of Texas at Austin indicates that the severity of the loading appears to increase significantly with Mach number.<sup>7</sup>

Such intense pressure fluctuations, driven by the self-sustaining vortex oscillation, can excite vibration of the local bay structure (or the store or missile components inside the cavity) and cause material failure. The oscillatory flowfield can also adversely affect the stable release of weapons. A characteristic of the oscillation cycle is the formation of shocks due to the impingement of the shear layer on the rear wall. The impingement causes high-energy flow to enter the cavity. As the cavity pressure increases above the freestream pressure, the shear layer is deflected out of the cavity which in turn causes the shock to disappear and the cavity "breathes out" mass with low momentum. There are currently two main models of the cavity oscillation process. Experiments<sup>1,8</sup> and computational analyses<sup>6,9</sup> indicate that as the shedding vortices are convected downstream from the cavity lip they get bigger. Due to the instability of these vortices, the shear layer deflects upward and downwards resulting in a shock/impingement event on the rear wall of the cavity. The shock impingement creates an acoustic wave which moves upstream at the local sound speed and impacts the front wall which in turn creates new shedding vortices. The second model was proposed by Heller and Bliss<sup>10</sup> who assume that the compression waves reflected from

---

\* Postdoctoral Fellow, Member AIAA

† Assistant Professor, Senior Member AIAA

‡ Professor, Associate Fellow AIAA

the front wall rather than the shedding vortices are the cause of the impingement event on the rear wall.

Rossiter<sup>1</sup> proposed an empirical formula to predict the oscillation frequency modes. This formula as modified by Heller et al.<sup>11</sup> is expressed as

$$Str = \frac{fL}{U} = \frac{n - \alpha}{M \sqrt{1 + 0.5\beta(\alpha - 1)M^2} + \frac{1}{k_c}}, n = 1, 2, 3, \dots$$

where  $n$  is the mode number inside the cavity,  $\beta$  is the recovery factor,  $\alpha$  is the phase shift function between vortex train and cavity acoustic waves, and  $k_c$  is an empirical parameter accounting for the ratio of the speed of convection of vortices to the freestream speed. While the oscillation frequencies for cavity flow may be predicted reasonably accurately by this empirical formula, no simple analytic formula can predict the associated amplitudes of the fluctuating pressure, nor can current Reynolds-Averaged-Navier-Stokes based computations predict them. To develop such a capability, there is a need for further detailed experimental investigations as well as computational ones.

There have been a considerable number of theoretical/numerical and experimental studies aimed at understanding various aspects of the cavity flow dynamics over a wide range of Mach numbers, from low subsonic to hypersonic. However, from an experimental perspective, the fraction of the literature dealing with unsteady hypersonic flowfields, is relatively small. Despite the extensive database, some fundamental aspects of the cavity oscillation cycle are not yet clear. For example, two outstanding questions that need to be answered are:

- 1) What is the real cause of the deflection of the shear layer? Is it the shedding vortices originating from the cavity front lip, or the compression waves reflected from the cavity front wall? Or, is there some sort of coupling between these two mechanisms?
- 2) What is the role of the incoming turbulent boundary layer in this process? Does the type of the individual boundary layer structure correlate with the deflection of the shear layer and hence the impingement of the shock?

### Objectives of Current Work

The current work represents preliminary results of an ongoing study in which the primary objective is to investigate the underlying physics of the high-speed

cavity flow dynamics using a combination of planar laser imaging techniques (including PLS and PIV) combined with fast response surface pressure measurements. It is believed that these techniques will provide detailed flowfield data which will lead to an improved understanding of the cavity dynamics. In addition to this, the data to be generated in the current study should be valuable in the validation of computational efforts such as large eddy simulation (LES) codes. For any confidence to be placed in simulation of turbulent flow over complex geometries (such as weapons bays of modern fighter aircraft), these techniques must first demonstrate that they can successfully model simpler cases.

In this first part of the study, reported in this paper, the goals were to demonstrate the PLS technique in the Mach 5 cavity flow with a particular emphasis on relating simultaneously acquired pressure signals to structures observed in the images. Specific issues of interest include the shock impingement process on the rear wall, the deflection of the shear layer in and out of the cavity, and the effects of the shear layer structures on the impingement process. These preliminary measurements will form the basis for later detailed PLS and PIV measurements which will include phase-average and real-time movies.

## Experimental Program

### Wind Tunnel and Flow Conditions

All of the experiments were conducted in the Mach 5 blowdown tunnel of the University of Texas at Austin. The constant-area test section is 6 in. (15.2 cm) wide by 7 in. (17.8 cm) high for this facility and has a length of 30 in. (76.2 cm). Removable side doors allow access to instrumented floor section. A total of about 140 ft<sup>3</sup> (4 m<sup>3</sup>) of compressed air is provided by a Worthington HB4 four-stage compressor and stored in external tanks at a pressure of about 2500 psia. Two 420 kW banks of nichrome wire resistive heaters located upstream of the stagnation chamber heat the incoming air to the desired stagnation temperature, which is measured by a Type J thermocouple. These heaters can provide stagnation temperatures of up to 759 °R (422 K). The stagnation chamber pressure and temperature for the present experiments are approximately 333 ± 3 psia and 635 °R, respectively. For these stagnation conditions, stable run times of up to 1 minute can be obtained. The nominal properties of the incoming freestream flow in the test section are given in Table 1.

The incoming turbulent boundary layer undergoes natural transition and develops under approximately adiabatic wall temperature conditions. The boundary layer thickness,  $d_b$ , is based on the height in the boundary layer where the local velocity reaches 99% of the freestream value. Values of basic parameters of the undisturbed turbulent boundary layer on tunnel centerline at approximately the location of the cavity model in the test section are given in Table 2.

Table 1 Incoming Flow Conditions

$M_\infty$	4.95	4.95
$U_\infty$	2509 ft/s	765 m/s
$Re_\infty$	$15.24 \times 10^6/\text{ft}$	$50 \times 10^6/\text{m}$
$P_0$	333 psia	$2.3 \times 10^6 \text{ N/m}^2$
$T_0$	635 °R	353 K

Table 2 Incoming Boundary Layer Parameters in the Mach 5 Test Section

$d$	0.76 in.	1.93 cm
$d$	0.36 in.	0.91 cm
$H \equiv d/q$	12	12
$\Pi$	0.44	0.44
$Re_q$	$3.8 \times 10^4$	$3.8 \times 10^4$
$C_f (\times 10^4)$	7.6	7.6

## Instrumentation and Data Acquisition

Fluctuating pressure measurements were made using Kulite Semiconductor Products, Inc., Model XCQ-062-15A and XCQ-062-50A transducers. These transducers have a nominal outer diameter of 0.0625 in. (0.159 cm) and a pressure-sensitive diaphragm of 0.028 in. (0.071 cm) in diameter. Perforated screens above the diaphragm protect the transducer from damage due to any dust particles in the flow but limit the frequency response of both models to about 50 kHz. The characteristic frequency of the larger shear-layer structures, on the other hand, is expected to be of order  $U_\infty/S$  where  $S$  is the structure spacing ( $1 - 2d_b$ ) which corresponds to a frequency of 25-50 kHz. The transducers were flush-mounted on two 3 in. (7.62 cm) wide by 1 in. (2.54 cm) high by 1 in. long blocks.

Output from the Kulite pressure transducers was amplified by either Dynamics (Model 7525), Vishay Measurements Group (Model 2311), or PARC (Model 113) amplifiers. The amplified signals were then filtered using Ithaco (Models 4113 or 4213) analog filters. A sampling rate of 200 kHz was used in all the experiments while the filter cut-off was set at 40 kHz. The signal-to-noise ratio was about 200.

Pressure data were acquired using two LeCroy analog-to-digital (A/D) converters with 12-bit resolution (Model 6810 waveform recorders). Each A/D converter has 4 megabytes of memory and can sample 1 channel of data at rates up to 5 MHz, or 4 channels of data simultaneously at rates up to 1 MHz per channel. The two A/D's can acquire data from 8 channels simultaneously when triggered using the same clock. For the current work, either 6 or 8 channels were used depending on the cavity model tested. For the cavity with L/H (length-to-depth ratio) = 6, two transducers recorded the pressure signal whereas always four transducers were used to record the pressure signal at the rear wall. The remaining two channels recorded the frame grabber and the laser Q-switch signals. For the fluctuating pressure measurements only, 524288 data points were acquired per channel with a sampling frequency of 200 kHz. For simultaneous pressure and PLS measurements 4096 data points per channel were acquired for each acquired PLS image. For simultaneous measurements the A/D converters were pre-triggered: once the frame grabber triggered the A/D, the A/D assigned the triggering time as the center of the total 4096 data points for each channel, and took 2048 data points before and after the triggering time. This way it was possible to avoid some synchronization problems due to the electronics and accurately match the timing of the image and pressure signals.

## Cavity Model

The cavity model which was used for the current study has a nominal height of 1 in. (2.54 cm) with a length that can be varied from 6 to 8 in. (15.2 to 20.3 cm). An assembly drawing of the main components of the cavity model is shown in Fig. 1. The cavity frame is flush-mounted in the tunnel floor and has a 3 in. (7.6 cm) wide by 8 in. (20.3 cm) long cut-out that forms the front, rear, and side walls of the cavity. The bottom plate is then used to form the cavity floor. On the centerline of the cavity floor there is a slot which is 0.25 in. (0.64 cm) wide and 6.9 in. (17.53 cm) long. This slot was designed for a glass window made out of fused silica which was anti-reflection coated on both sides. The idea was that

the use of fused silica would allow the laser sheet to pass through and thereby reduce the background scattering problem from the floor and side walls of the cavity in the PLS experiments. The cavity floor and the fused silica are both 0.5 in high. The fused silica is tapered with a 60 degree angle with the horizontal plane and is held in the slot through two support plugs of the same width at both ends. These support plugs were used to prevent the suction of the fused silica into the freestream. A second narrow plate which also has a slot (to allow the laser sheet pass through) was used underneath to support the fused silica, and to hold the support plugs in place. The PLS experiments proved that the use of fused silica solved the background scattering problem quite successfully. Two 1 in. blocks from the previous cavity model which was used in previous work<sup>7,12,13</sup> are also used with this new cavity. These 1 in. blocks have ports for pressure transducers and can be placed in the upstream and downstream ends of the cavity (Fig. 2). The intent is to use the rear transducer block to monitor the shear layer impingement (and subsequent bow-shock generation) at the top of the rear wall. The front wall transducers are mainly needed to calculate the space-time correlations between the front and rear wall pressure signals especially to examine the propagation of the acoustic wave which is linked to the shear layer impingement. With the rear block in place a maximum nominal L/H ratio of 7 can be obtained. With these L/H ratios, the nature of the cavity flow is an "open" type. An "open" type of cavity is one in which the separated shear layer bridges the cavity and reattaches onto the downstream face of the cavity.

### Planar Laser Scattering

The PLS imaging relies on the scattering from a fine ethanol fog that results from the condensation of ethanol directly injected into the plenum section using three fine spray atomizing nozzles (Spraying Systems LN30).<sup>14,15</sup> The ethanol was supplied using a stainless steel reservoir of capacity 2 ft<sup>3</sup> (0.057 m<sup>3</sup>) which is pressurized to 600-750 psia (4.1-5.2x10<sup>6</sup> N/m<sup>2</sup>). The flow then passes through a fine mesh screen before entering the plenum.

Optical access through the side of the test section is provided by a fused silica window which is 6 in. (15.2 cm) long by 2 in. (5.1 cm) high by 0.75 in. (1.9 cm) thick. A narrow acrylic window, 9 in. (22.9 cm) long by 0.5 in. (1.27 cm) wide by 0.75 in. (1.9 cm) thick, provides access for the laser sheet through the top of the test section. Side view images are obtained by passing the laser sheet vertically through the top window while

the camera views through the side window at 90 degrees to the sheet.

A schematic diagram of the PLS imaging setup is shown in Fig. 3. An Nd:YAG laser (Spectra-Physics GCR-150) is the light source of the system. The laser is frequency doubled to 532 nm and operates at 10 Hz. For the current experiments the Nd:YAG laser provided about 35 to 55 mJ per pulse. The laser beam was formed into a sheet approximately 5.5 in. (14 cm) wide and 250  $\mu$ m thick using a spherical and cylindrical lens. The scattering was imaged using a CCD video camera (Cohu 4990). The images were digitized using a frame grabber (DataTranslation DT2851) installed in a 486 IBM compatible PC with sufficient memory to store 90 images of resolution 240x512. The image processing was done using the Khoros 1.0 image processing package.

## Results

### Oscillatory Mode Frequencies

The power spectra for the uppermost transducer on the rear wall [0.125 in. (0.318 cm) inside the cavity (RW7)] are plotted in Fig. 4 for four L/H ratios. The cases L/H=3 and 4 are from Ref. 12. In the figure the spectra are presented in the nondimensional form as sound pressure level (SPL) versus Strouhal number. Comparison of the power spectra shows that as L/H increases, the overall power level increases for all frequencies, and that the spectra become more broadband (or the spectral peaks become less distinct). This result is expected since the shear layer impingement occurs closer to the cavity floor on the rear wall with increasing L/H and consequently higher-energy fluid enters the cavity thus increasing the local pressure oscillations.

The power spectra for the uppermost transducer on the front wall [0.125 in. (0.318 cm) inside the cavity (FW1)] are plotted in Fig. 5 for L/H=3, 6 and 7. The L/H=3 case is from Ref. 13. Note that the mode frequencies are more evident in the front wall power spectra. This is because the "noise" level near the rear wall is increased by the unsteady impingement shock at the top edge of the rear wall. Examination of the spectra shows that the first two oscillatory modes occur approximately at the same Strouhal number while this is not true for the third and fourth modes. For the first mode the power level increases as L/H increases, whereas for the second mode the power level for the shorter cavity is not only higher but also sharper. For cavities with L/H=6 and 7 the third mode is less prominent while it is very distinct in the case of L/H=3. The mode frequencies from the experiments for the first four modes and the

corresponding calculated values based on Rossiter's improved formula are given in Table 3. The calculated values were found using two different sets of  $k_c$  and  $\alpha$ . The first set ( $k_c=0.65$  and  $\alpha=0.3$ ) is based on the average value of  $k_c$  and  $\alpha$  from earlier work<sup>1,5,16</sup> whereas the second set is based on the interpretation of Heller and Bliss,<sup>10</sup> in which case  $k_c$  is defined as the ratio of "the adiabatic temperature sound speed in the cavity" to "the freestream speed." Examination of Table 3 shows that the experimental values of mode frequencies are predicted quite well with the first set of  $k_c$  and  $\alpha$ .

Table 3 Experimental and calculated mode frequencies

L/H	n freq. modes	$\frac{fL}{U_\infty}$ experimental	$n - a$	
			$\frac{M}{\sqrt{1+0.5b(g-1)M^2}} + \frac{1}{k_c}$	
			$k_c=0.65$ $\alpha=0.3$	$k_c=0.4682$ $\alpha=0$
6	1	0.17 - 0.23	0.19	0.23
6	2	0.41 - 0.45	0.46	0.47
6	3	0.72 - 0.76	0.73	0.70
6	4	0.98 - 1.04	1.01	0.94
7	1	0.16 - 0.21	0.19	0.23
7	2	0.40 - 0.45	0.46	0.47
7	3	0.70 - 0.75	0.73	0.70
7	4	1.04 - 1.10	1.01	0.94

### Characteristics of Shock Impingement Process

The normalized cross-correlation between the pressure signals on the front wall (FW1) and rear wall (RW7) transducers is presented in Fig. 6. The time is normalized by  $L/U_\infty$  where  $U_\infty$  is the freestream velocity and  $L$  is the cavity length. For comparison the result of Ref. 13 ( $L/H=3$ ) is included and shows that the highest peak value of the cross-correlation for the FW1 and RW7 is 0.159 and occurs at  $tU_\infty/L=-2.138$  (Fig. 6a). Since the normalized time for an acoustic wave to travel from the rear wall to the front wall is 2.133 assuming stagnant fluid in the cavity, this suggests that the cause of the peak at  $tU_\infty/L=-2.138$  is such an acoustic wave. The results of the current work for  $L/H=6$  supports this conclusion: the peak values of the cross-correlation of the FW1 and RW7 signals are 0.086 and 0.122, and occur at  $tU_\infty/L=\pm 2.108$ , respectively. Assuming that these peak values in the cross-correlation are due to the same cause (i.e., acoustic wave), the

normalized period would be  $TU_\infty/L=4.216$ . The corresponding Strouhal number of the first mode frequency is then calculated as 0.237 which is close to the experimental value of the first mode given in Table 3. Another observation stemming from the similarity of the cross-correlation curves of these two cases is that the overall flow structure causing the correlation between the front and the rear wall pressure signals is the same.

The highest peak value of the cross-correlation of FW1 and RW1 [0.125 in. (0.318 cm) above the cavity floor] signals for  $L/H=3$  is 0.310 and occurs at  $tU_\infty/L=-1.948$ , whereas in the case of  $L/H=6$  these values are 0.505, and -2.008, respectively (Fig. 6b). As expected, the cross correlation curves are also very similar in this case. Compared to the shorter cavity, the peak value of the correlation between FW1 and RW7 is smaller whereas the peak value between FW1 and RW1 is larger by 63%. The increase in the cross-correlation is quite probably due to the increased amount of high energy fluid inside the cavity: for a longer cavity, the impingement of the shear layer on the rear wall occurs closer to the cavity floor, and consequently stronger pressure oscillations are generated.

In this first part of the study one of the goals was to determine some of the characteristics of the shock impingement process through simultaneous measurements of pressure and PLS imaging. These preliminary measurements and analysis will form the basis for the detailed measurements in the second part which will include phase-average and real time movies. Two features of the impingement shock behavior which are important in understanding the cavity oscillation cycle are the duration of the shock,  $t_d$ , and the delay between two consecutive shock events,  $T_s$ . To determine these characteristics, the pressure signal from the uppermost transducer on the rear wall (RW7) was analyzed for three different  $L/H$  ratios (namely, 3, 6, and 7). Fig. 7a shows the first 1000 points of the pressure history for the  $L/H=6$  case. The threshold value for detecting a shock "event" was chosen as  $P_m = P_m + 2.5S$  where  $P_m$  and  $S$  are the mean and standard deviation of the pressure signal, respectively. The resulting boxcar signal (Fig. 7b) was then calculated to find the shock events. Based on the boxcar signal, the duration of an event  $t_d$  was calculated as  $t_1-t_2$  where  $t_2$  refers to the time when the value of the pressure signal exceeds the threshold, and  $t_1$  refers to the time when the value of the signal decreases below the threshold. The time between two consecutive shock events was determined as  $t_2-t_{2p}$  where  $t_{2p}$  refers to the starting point of the previous shock

event. Based on these definitions the average values of  $t_d$  and  $T_s$  can be found from

$$t_m = \overline{t_d} = \sum_{k=1}^N (t_1 - t_2) / N$$

$$T_m = \overline{T_s} = \sum_{k=1}^N (t_2 - t_{2p}) / N$$

where  $N$  is the total number of shock events. Values of the average shock duration time,  $t_m$ , for different L/H ratios are plotted in Fig. 7c. From the figure it can be seen that  $t_m$  does not seem to be sensitive to the cavity length-to-depth ratio, and varies between 20-30  $\mu$ s. This time scale is of order that required for a large-scale shear layer structure to convect past a given point. The average time delays between two consecutive shocks,  $T_m$ , for the same cases are shown in Fig. 7d. Again, there is no definitive trend but the value is in the range of 0.7 to 1 ms. The corresponding frequency range of the impingement shock is 1-1.4 kHz. The histogram for  $T_s$  is shown in Fig. 7e. The distribution of  $T_s$  in the histogram does not reveal a significant peak which in turn shows that the shock event does not seem to be periodic.

### Side View PLS Images

Three different cavity configurations, namely L/H=6, 7, and 8 were used. Because the glass window on the side door of the test section was shorter than the smallest cavity length, it was necessary to visualize the rear wall location and the middle region of the cavity separately. When necessary, the camera was given slight angles in the horizontal plane. Since these angles were small, the sharpness of the images was not affected in general. Of the three cavity configurations tested, it was possible to acquire pressure data simultaneously for two cases: in the case of L/H=6, the front and rear wall transducer blocks were used, whereas for L/H=7 only the rear block could be used.

Fig. 8 shows the instantaneous side view PLS image around the rear wall location (Fig. 8a) along with the pressure signals from the uppermost rear (RW7) and front (FW1) wall transducers (Fig. 8b). The field of view starts from 3 in. (7.6 cm) upstream of the rear wall on the left and extends to 1 in. (2.54 cm) downstream of the rear wall on the right. The flow is from left to right for all images. This particular image has a large shear layer structure just in front of the rear wall. A weak compression wave can be seen originating from the upstream edge of the structure. An impingement shock does not exist at this particular instant. The pressure

signal in the figure spans 2 ms in time, centered at the time the image was taken. The thick vertical line indicates the time at which the image was taken. Assuming that the shear layer structures convect with 80% of the freestream velocity, the convection time for a structure to span a 4 in. (10.2 cm) distance (i.e., the streamwise length of the field of view in the image) is about 166  $\mu$ s which is shown as a thick horizontal line in Fig. 8b. Note that the pressure signal on the rear wall (RW7) is quite intermittent, whereas the front wall (FW1) signal is quite steady. At the time of the image acquisition the pressure signal on the rear wall has a small peak but compared to the overall signal the peak value does not represent one of the significant peaks. The absence of a shock, the large structure and the compression wave, and the pressure signal suggest that the cavity may be “breathing out” fluid.

In statistical terms the impingement shock was visualized in approximately one third of the images taken for the current study. One sample PLS image and the corresponding pressure signals are given in Fig. 9. The shear layer is quite active and the shock on the rear wall is clearly visible. Even though the corresponding RW7 pressure signal does not show a clear peak, the pressure is high compared to the overall signal.

Fig. 10a shows a conditionally acquired instantaneous PLS image for a cavity with L/H=7. The field of view for this case is about 5 in. (12.7 cm) and from 4 in. (10.16 cm) upstream of the rear wall on the left and extends to 1 in. (2.54 cm) downstream of the rear wall on the right. The impingement shock on the rear wall can be clearly seen as well as the expansion wave emanating from the upstream region. The signal from the uppermost transducer (RW7) at the rear wall is also recorded by the frame grabber and its voltage value is compared with a threshold voltage value of the frame grabber which is set by the user. When the signal value exceeds the threshold, the frame grabber triggers the A/D for the pressure data acquisition and the flashlamp for the image acquisition. The PLS image is acquired at the time of the laser pulse as indicated by the thick vertical line in the image. For this particular case the acquired pressure signal is shown in Fig. 10b. Note that the higher pressure values recorded by the uppermost transducer on the rear wall suggest that the impingement shock is stronger for this longer cavity, which is expected. The pressure data for this case was expanded and covers a segment of 1 ms. At the time of the acquisition the pressure is high even though is not exactly at its peak value. The time for a shear layer structure to pass the image window is about 207  $\mu$ s and shown in Fig. 10b as the horizontal thick line.

A sample PLS image for the longest cavity ( $L/H=8$ ) is shown in Fig. 11. The field of view for the image is given underneath. This was the only case where the camera had to be given a large angle (30 deg.) to visualize the rear wall. Therefore, not only the field of view is shorter (4 in.) but also the sharpness on the upstream part of the image was affected. Nevertheless, the impingement shock is still visible.

Charwat *et al.*<sup>17</sup> estimated the critical ratio of  $L/H$  to be about 10 beyond which the shear layer attaches on the cavity floor leaving two separated flow regions near the front and rear walls. Therefore, the expectation was that the deflection of the shear layer into the cavity would be visible with the longer cavity models. Fig. 12a presents such an instantaneous PLS image for the longest cavity ( $L/H=8$ ). The corresponding field of view is given in Fig. 12b. The shear layer seems to be deflecting into the cavity, and as a result an expansion wave develops which can be recognized from the darker region behind it.

Ensemble-average images were also obtained for all the configurations tested. Ninety images were used for the ensemble averaging. When the focus was on the rear wall, the shock was clearly visible in the ensemble-average images, and when the focus was in the middle region of the cavity the expansion waves were also clearly visible (not shown). It was also observed that as the length of the cavity was increased the location of the expansion wave moved upstream. This observation is an indication that the shear layer starts deflecting into the cavity after a certain distance downstream of the front wall (about 2.5 in.). Even though there were clues in some of the instantaneous images that the shear layer deflects into the cavity, most of the time the structures on the outer part of the shear layer masked the deflection. Consequently, the deflection was not visible from the shear layer thickness at both ends of the field of view. Considering the mass-in/mass-out cycle of the cavity, there are times that the high-momentum fluid enters the cavity causing the deflection of the shear layer into the cavity, and times when the cavity breathes out the mass, in which case the shear layer may be expected to get thicker inside the cavity. The overall effect in an ensemble-average image might be such that these two processes may cancel out each other. In the absence of the time history of the shear layer over the cavity it would be premature to reach any conclusions based on these ensemble-average and instantaneous images.

## Summary

Simultaneous Planar Laser Scattering (PLS) imaging and fluctuating pressure measurements have been made

for a rectangular cavity in a Mach 5 turbulent boundary layer. Preliminary results are presented in the form of instantaneous side view images, and power spectra for cavity length-to-depth ratios of 3, 4, 6, 7, and 8. High-frequency response pressure transducers were installed in the rear and front walls of the cavity to monitor the shear layer impingement at the top of the rear wall, and to determine the upstream propagation time of acoustic waves from space-time-correlations. Instantaneous side view PLS images show the impingement shock and expansion waves, whereas the large turbulent structures at the outer edge of the shear layer mask the deflection of the shear layer into the cavity, even for the largest cavity tested. Preliminary analysis of the fluctuating pressure data suggests that the shock frequencies and the duration of the impingement shock are not sensitive to cavity length-to-depth ratio.

## Acknowledgment

Support for this research has been provided through a grant from Air Force Office of Scientific Research (F49620-97-1-0060) monitored by Drs. L. Sakell and S. Walker. The authors gratefully acknowledge this support.

## References

- <sup>1</sup>Rossiter, J. E., "Wind-Tunnel Experiments on the Flow Over Rectangular Cavities at Subsonic and Transonic Speeds," A.R.C.R. & M., No. 3438, 1964.
- <sup>2</sup>Maurer, O. F., "Investigation and Reduction of Open Weapon Bay Pressure Oscillations Expected in the B-1 Aircraft," AFFDL TM 74-101, 1973.
- <sup>3</sup>Rockwell, D., and Naudascher, E., "Review—Self-Sustaining Oscillations of Flow Past Cavities," *ASME J. Fluid Engr.*, Vol. 100, 1978, pp. 152-165.
- <sup>4</sup>Stallings, Jr. R. L., "Store Separation from Cavities at Supersonic Flight Speeds," *J. Spacecraft*, Vol. 20, 1983, pp. 129-132.
- <sup>5</sup>Zhang, X., and Edwards, J. A., "An Investigation of Supersonic Oscillatory Cavity Flows Driven by Thick Shear Layers," *Aeronautical Journal*, 1990, pp. 355-364.
- <sup>6</sup>Rizzetta, D. P., "Numerical Simulation of Supersonic Flow Over a Three-Dimensional Cavity," *AIAA Journal*, Vol. 26, 1988, pp. 799-807.
- <sup>7</sup>Perng, S. W., and Dolling, D. S., "Passive Control of Pressure Oscillations in Hypersonic Cavity Flow," AIAA Paper 96-0444, Jan. 1996.

- <sup>8</sup>Pereira, J. C. F., and Sousa, J. M. M., "Experimental and Numerical Investigation of Flow Oscillations in a Rectangular Cavity," *ASME J. Fluid Engr.*, Vol. 117, 1995, pp. 68-74.
- <sup>9</sup>Morgenstern, Jr. A., and Chokani, N., "Hypersonic Flow Past Open Cavities," AIAA Paper 93-2969, 1993.
- <sup>10</sup>Heller, H. H., and Bliss, D. B., "The Physical Mechanism of Flow-Induced Pressure Fluctuations in Cavities and Concepts for Their Suppression," AIAA Paper 75-491, 1975.
- <sup>11</sup>Heller, H. H., Holmes, G., and Covert, E. E., "Flow-Induced Pressure Oscillations in Shallow Cavities," AFFDL-TR-70-104, Dec. 1970.
- <sup>12</sup>Perng, S. W., "Passive Control of Pressure Oscillations in Hypersonic Cavity Flow," Ph. D. Dissertation, Dept. of Aerospace Engineering and Engineering Mechanics, The University of Texas at Austin, Austin, TX, Dec. 1996.
- <sup>13</sup>Leu, Y. L., and Dolling, D. S., "Passive Control of Pressure Oscillations in Cavity Flow with Store Release," Proc. of Wind Tunnels and Wind Tunnel Test Techniques, The Royal Aeronautical Society, Cambridge, UK, Apr. 1997.
- <sup>14</sup>Chan, S. C., Clemens, N. T., and Dolling, D. S., "Flowfield Imaging of Unsteady, Separated Compression Ramp Interactions," AIAA Paper 95-2195, June 1995.
- <sup>15</sup>Beresh, S. J., Clemens, N. T., Dolling, D. S., and Comminos, M., "Investigation of the Causes of Large-Scale Unsteadiness of Shock-Induced Separated Flow Using Planar Laser Imaging," AIAA Paper 97-0064, Jan. 1997.
- <sup>16</sup>Kaufman, L. G. II, Maciulaitis, A., and Clark, R. L., "Mach 0.6 to 3.0 Flows Over Rectangular Cavities," AFWAL-TR-82-3112, 1982
- <sup>17</sup>Charwat, A. F., Roos, J. N., Dewey, Jr. F. C., and Hitz, J. A., "An Investigation of Separated Flows — Part I: the Pressure Field," *J. Aero. Sciences*, Vol. 28, 1961, pp. 457-470.

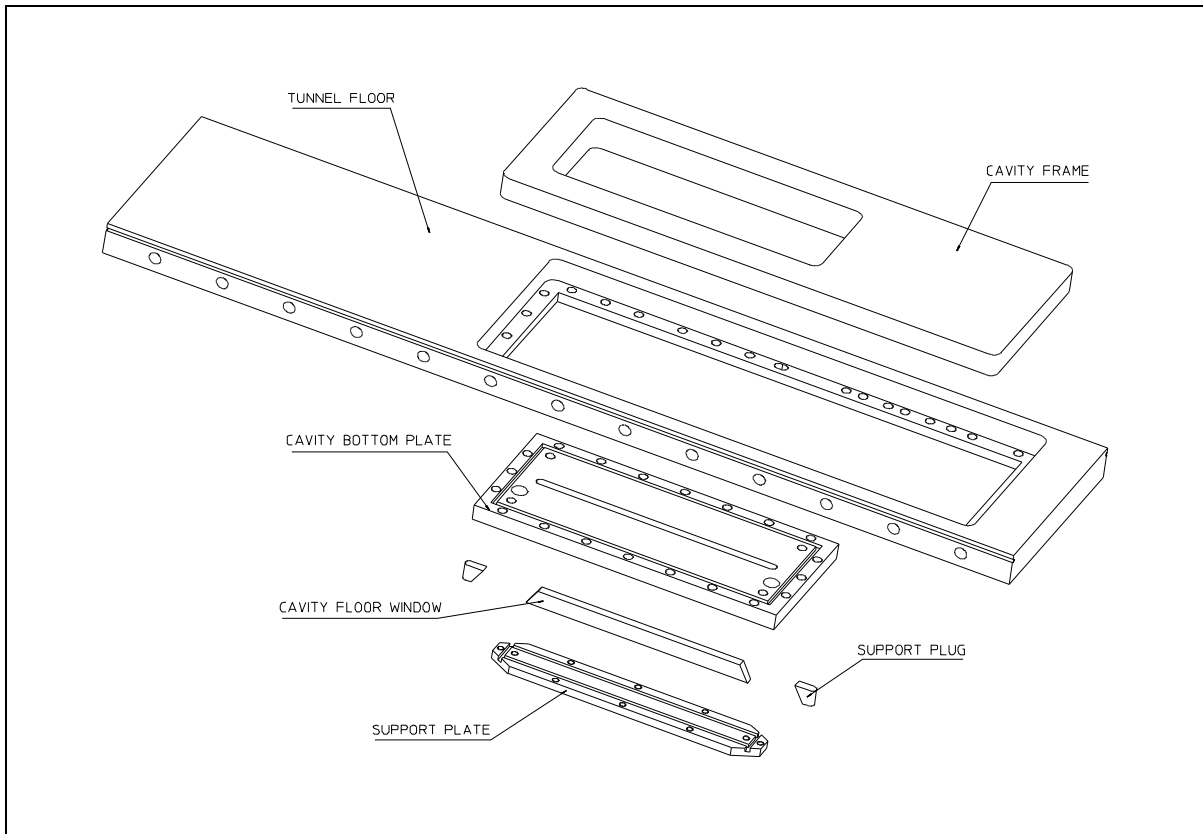


Fig. 1 Cavity Assembly

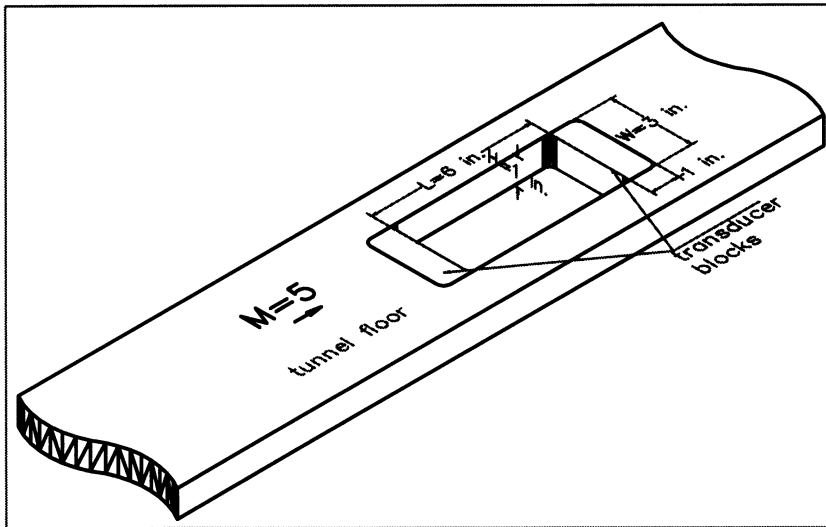


Fig. 2 Cavity geometry and transducer blocks

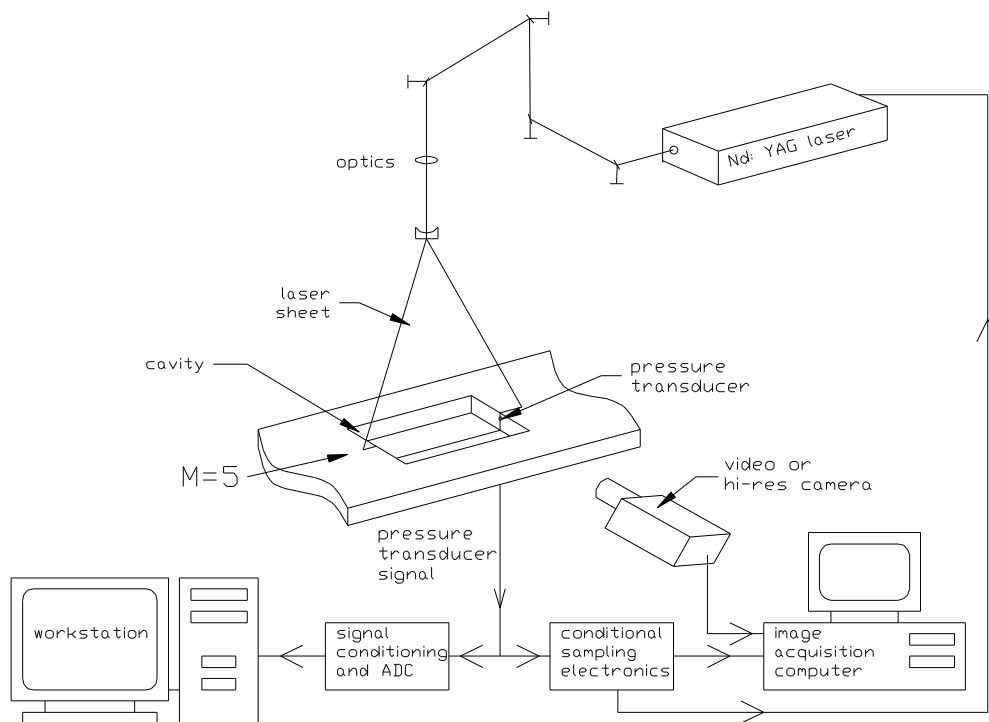


Fig. 3 Experimental setup for PLS imaging of the supersonic cavity flow

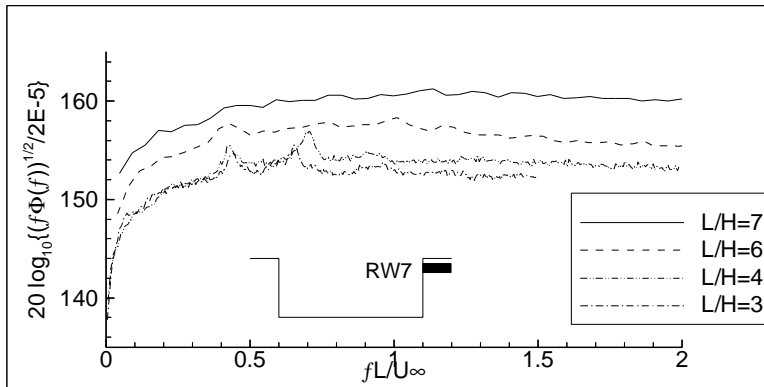


Fig. 4 Power spectra for the uppermost rear wall transducer (RW7)

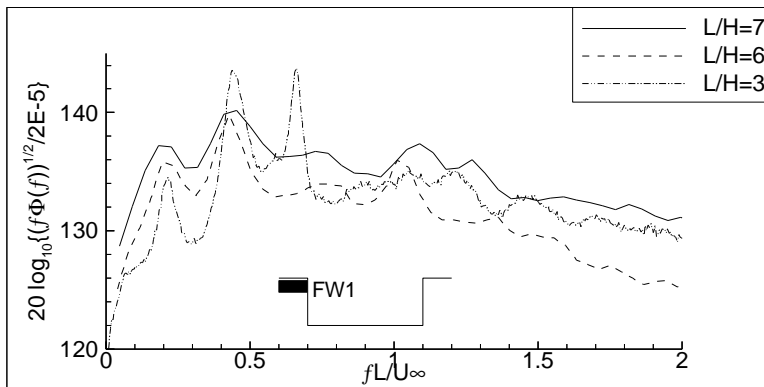
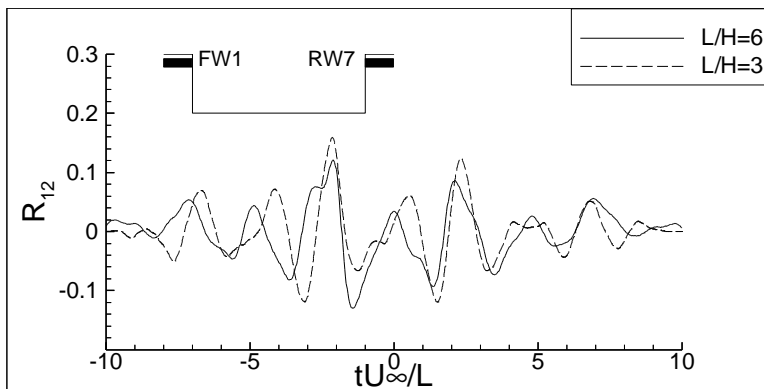
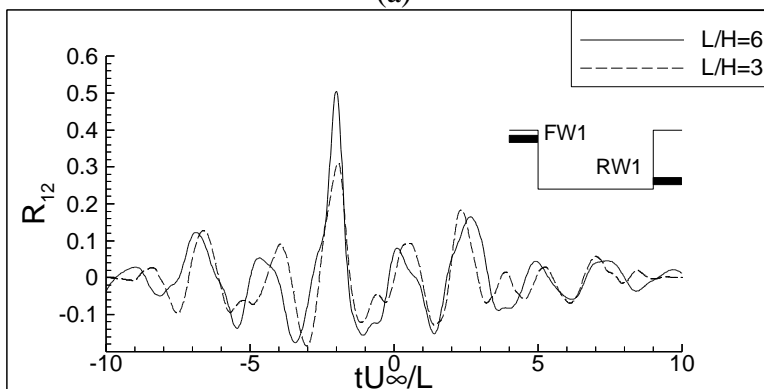


Fig. 5 Power spectra for the uppermost front wall transducer (FW1)

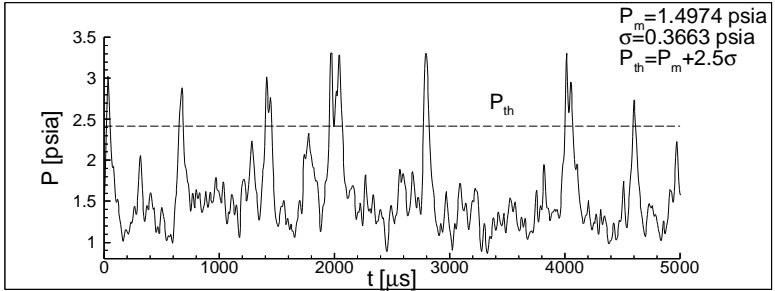


(a)



(b)

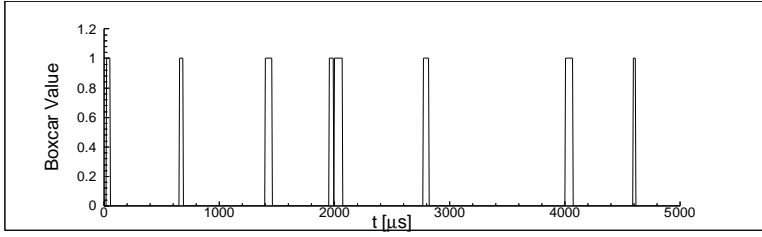
Fig. 6 Normalized cross-correlation of the pressure signals  
a) FW1 & RW7  
b) FW1 & RW1



(a)

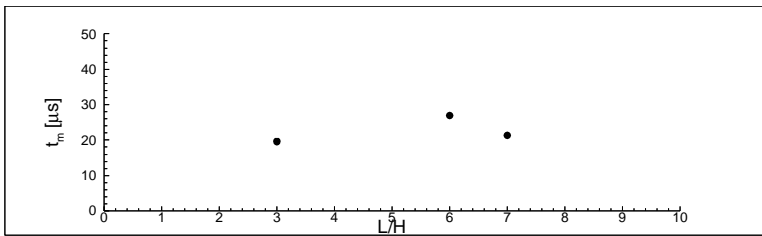
Fig. 7 Shock impingement analysis

a) Pressure data at RW7 for L/H=6



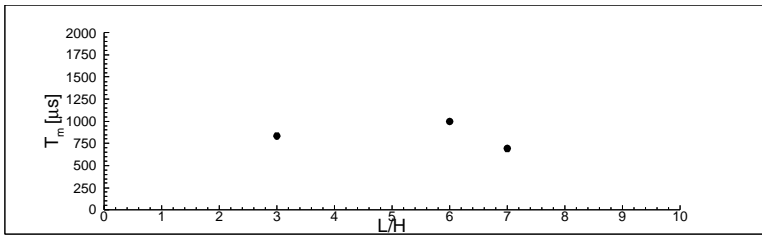
(b)

b) Corresponding boxcar signal



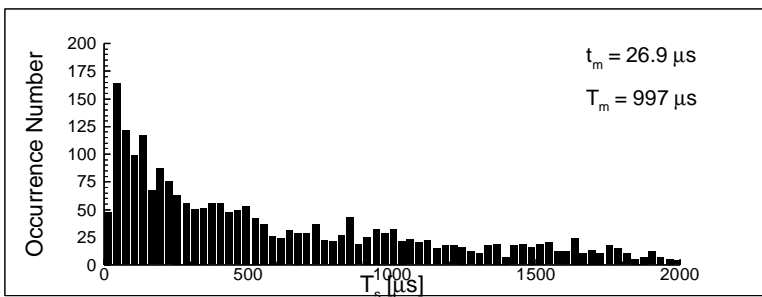
(c)

c) Average shock duration



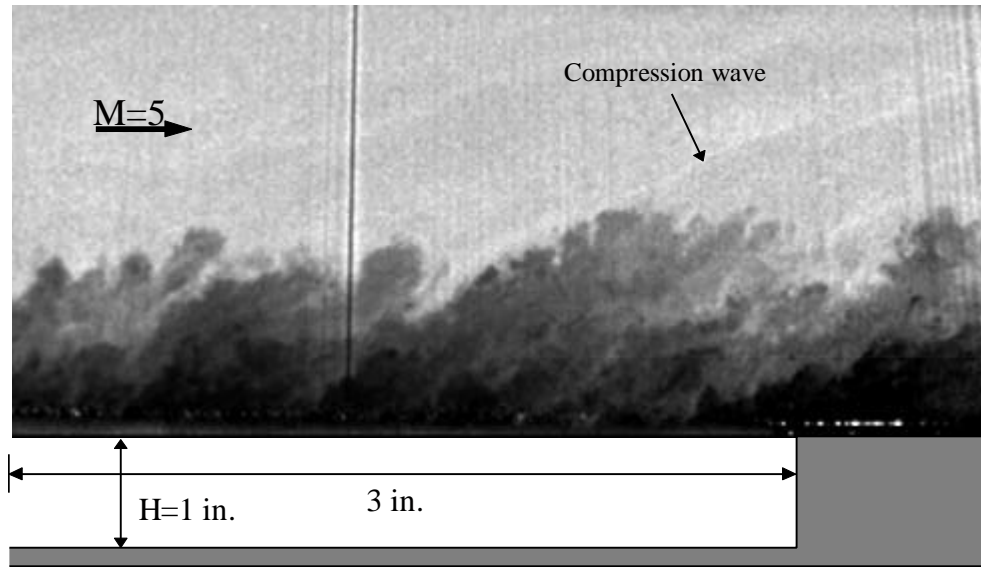
(d)

d) Average time delay

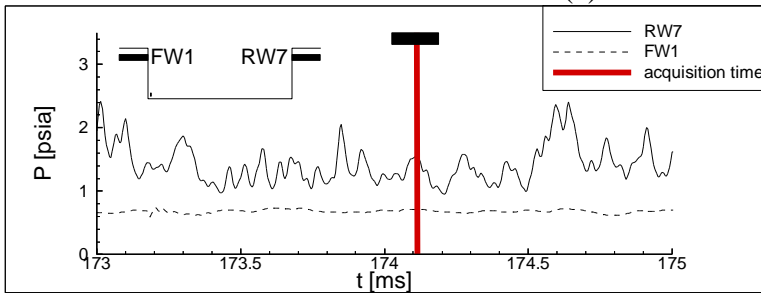


(e)

e) Time delay histogram for L/H=6

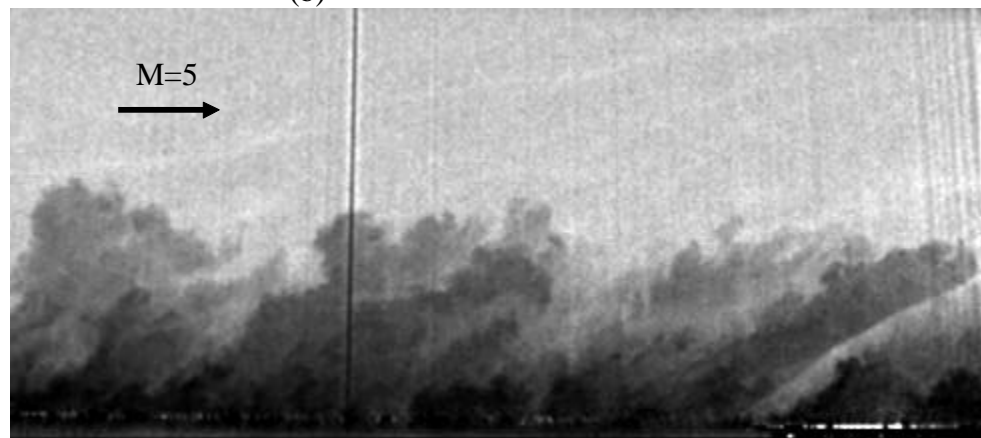


(a)

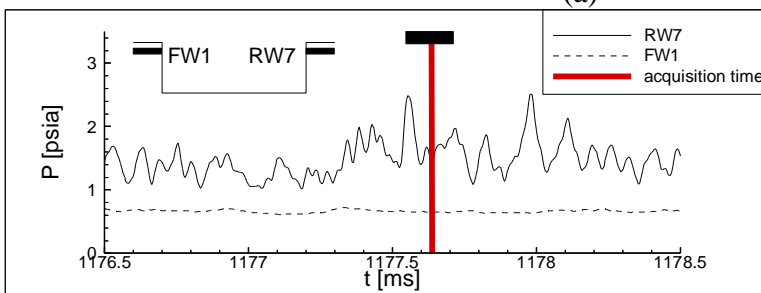


(b)

Fig. 8 Sample PLS image showing a large scale structure ( $L/H=6$ )  
 a) PLS image  
 b) Rear and front wall pressure signals

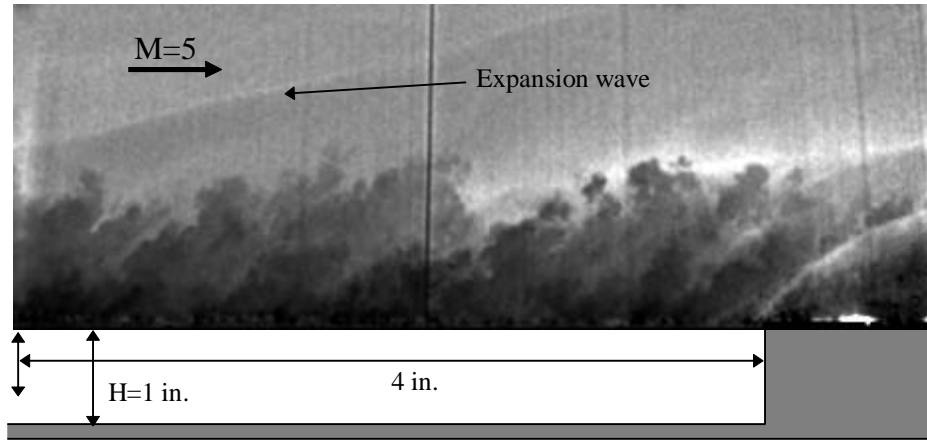


(a)

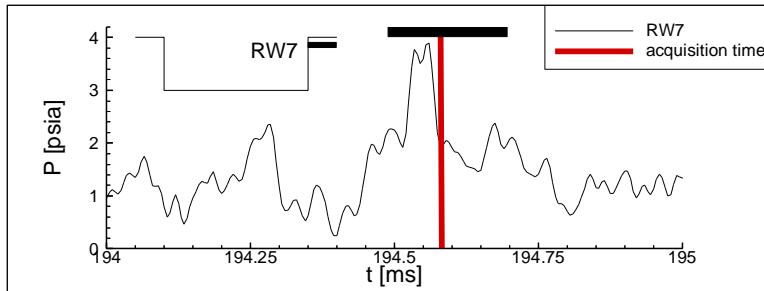


(b)

Fig. 9 Sample PLS image showing an impingement shock ( $L/H=6$ )  
 a) PLS image (field of view is the same as in Fig. 8a)  
 b) Rear and front wall pressure signals



(a)



(b)

Fig. 10 Conditionally acquired sample PLS image showing an impingement shock ( $L/H=7$ )  
 a) PLS image  
 b) Rear wall pressure signal

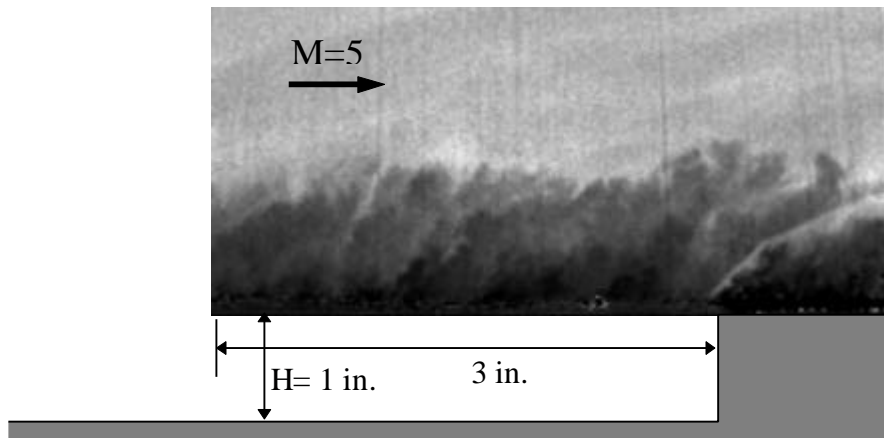
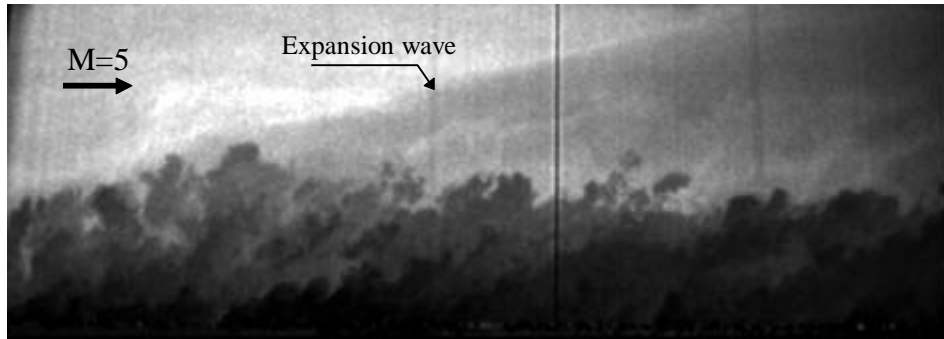
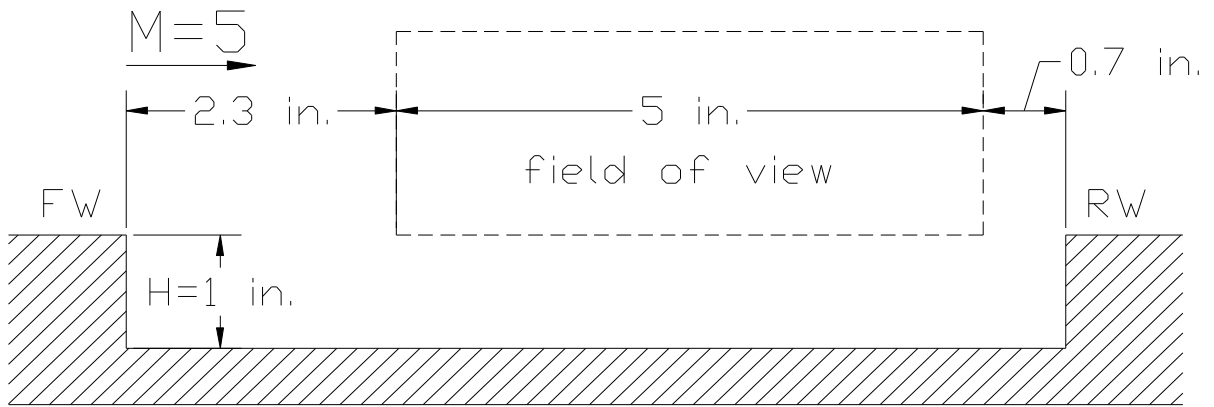


Fig. 11 Sample instantaneous side view PLS image for  $L/H=8$ .



(a)



(b)

Fig. 12 Sample PLS image showing the expansion wave ( $L/H=8$ )  
 a) PLS image, and b) Field of view